ISSN: 1813-162X (Print) ; 2312-7589 (Online)

Tikrit Journal of Engineering Sciences

available online at: http://www.tj-es.com

College of Engineering

TJES
Tikrit Journal of Engineering Sciences

Total Head Evaluation using Exact and Finite Element Solutions of Laplace Equation for Seepage of Water under Sheet Pile

Aram Mohammed Raheem *

Department of Civil Engineering
College of Engineering
Kirkuk University
Kirkuk
Iraq

***Keywords*:**

Laplace equation
Fourier series
FEM
total Head
seepage
sheet pile

A R T I C L E I N F O

Article history:

Received 27 February 2018
Accepted 13 June 2018
Available online 01 September 2018

A B S T R A C T

In this study, the strong and weak forms of Darcy flow equation has been derived. The final obtained equation is Laplace partial differential equation. For total head evaluation, Laplace equation is solved using exact solution depending on Fourier series and numerical solution depending on finite element method. A computer program has been developed in MATLAB program to solve the Laplace equation using both exact and finite element solutions and the seepage of water under sheet pile is taken as a case study. Different number of points and nodes has been selected for the two methods. It is shown that both exact and finite element solutions have a good match in distribution for the study area especially when the Fourier points are increased.

DOI: http://dx.doi.org/10.25130/tjes.25.3.07

تقييم الجهد الكلي باستخدام الحل الجبري الدقيق والعناصر المحددة لمعادلة لابلاس لتسرب المياه تحت الركيزة اللوحية

الخلاصة

تمت في هذه الدراسة اشتقاق الصيغ الاساسية المعروفة بالصيغ القوية والضعيفة لمعادلة دارسي الخاصة بالجريان. حيث ان الصيغة النهائية تمثل المعادلة التفاضلية الجزئية المعروفة بمعادلة لابلاس. لغرض حساب الجهد الكلي، تم حل معادلة لابلاس باستخدام الطريقة الرياضية الجبرية بالاعتماد على متسلسلة فورير وباستخدام الطريقة العددية بالاعتماد على طريقة العناصر المحددة. تم كتابة برنامج متكامل في الماتلاب لغرض حل معادلة لابلاس باستخدام الطريقتين وتم تطبيق الحلول على حالة تسرب المياه تحت الركائز اللوحية. تم دراسة تاثير عدد مختلف من نقاط فورير على الحل الجبري وكذلك تاثير عدد النقاط او العقد على الحل العددي في طريقة العناصر المحددة. وقد بينت الدراسة ان كل من الحل الجبري والحل العددي المتمثل في طريقة العناصر المحددة متقاربة في التوزيع على منطقة الدراسة وبالخصوص عند زيادة عدد نقاط فورير الخاصة بالحل الجبري.

1. INTRODUCTION

Sheet pile is one of the retaining structures that is mainly affected by the seepage of water underneath its base. The seepage of the water may alter the value and the distribution of the passive pressure where failure could happen at the base of the sheet pile due to the extreme difference in hydraulic head between the up and downstream [1].

When an excavating is complete in a huge area, the soil failure due to seepage in the front of the sheet pile is a problem in two dimensions where such problem was first addressed by Terzaghi [2].

A simple relation was proposed by Henry Darcy in (1856) using a laboratory experiment that is known by Darcy's law. Henry Darcy was the first to work in evaluating the amount of seepage in a homogenous soil and finally the Laplace partial differential equation of flow is obtained [3]. The Laplace flow equation was solved using exact solution depending on the method of separation of variables. Later on and after a half of century of advancement, finite element method (FEM) has used as a very powerful method for numerical computations in both engineering and science.

In the FEM, isoparametric elements are mapped elements that play a very important role in such numerical evaluation [4]. In numerical simulation, the determinant of

* *Corresponding author: E-mail* : engaram@yahoo.com

Nomenclature

$\underline{g}$	acceleration
h	the head of water
k	permeability coefficient
n	no. of points in the Fourier series
$\underline{n}$	unit normal vector
p	pressure
p_o	prescribed values of pressure on the boundary
$\underline{v}$	velocity
v_o	prescribed values of velocity

Greek symbols

μ	dynamic viscosity
ρ	density
Γ^N	Neumann boundary condition
Γ^D	Dirichilet boundary condition
$[\underline{K}]$	$\int_\Omega \left(\underline{\mathrm{B}}^{\mathrm{T}}\Theta\underline{\mathrm{I}}\right)^{\mathrm{T}}\left(\underline{\mathrm{B}}^{\mathrm{T}}\Theta\underline{\mathrm{I}}\right) d\Omega$
$[\underline{U}]$	$\mathrm{vec}\left[\underline{\mathrm{h}}^{\mathrm{T}}\right]$
$[\underline{F}]$	$-\int_\Omega \left(\underline{\mathrm{N}}\Theta\underline{\mathrm{I}}\right)^T \mathrm{vec}\left[\underline{\mathrm{B}}^{\mathrm{T}}\right]^T \mathrm{vec}\left[\underline{\mathrm{F}}^{\mathrm{T}}\right] \mathrm{d}\Omega$

the Jacobian matrix has to be checked continuously for its positivity in order to prevent distorted elements. Moreover, using Galerkin weak form for the numerical integration, Gauss quadrature is a frequently applied technique. Quadrature rule is necessary for problems with high-order approximated function that noticeably increase the computational cost in addition to the complexity in implementation [5]. Furthermore, the presence of modern computer program such as MATLAB is considered as a useful implement to solve well-defined problems encountered in geotechnical practice. Using MATLAB is beneficial in terms in dealing with such problems to obtain precious results speedily and accordingly to perform parametric investigations rapidly to be useful in the design perspective [6]. Hence, this study has focused in deriving all the necessary equations for total head evaluation with performing a comparative study on sheet pile using both exact and finite element methods.

The overall objective of this study was to evaluate the total head using both exact and finite element solutions of Laplace partial differential equation in the case of seepage of water under sheet pile. The specific objectives were as follows:

1- Develop a computer program in MATLAB to apply both exact and finite element solutions.
2- Investigate the contours of total head distribution over the studied area for both exact and finite element solutions.
3- Study the absolute error of the total head at every single node.

2. MATHEMATICAL BACKGROUND AND METHODS

2.1. Darcy Law

Darcy law can be given as below:

$$\underline{v} = -\frac{k}{\mu}\left(\mathrm{grad}[p] + \rho\underline{g}\right) \tag{1}$$

For incompressible fluid:
$\mathrm{div}\,[\,\underline{v}\,] = 0$, then

$$\mathrm{div}\,[\,\underline{v}\,] = \mathrm{div}\left[-\frac{k}{\mu}\left(\mathrm{grad}[p] + \rho\underline{g}\right)\right] = 0 \tag{2}$$

2.2. [S] or Strong Form

Use Eq. (2) to derive [S] problem:

$$-\mathrm{div}[\frac{k}{\mu}\,\mathrm{grad}(p)] = -\mathrm{div}\,[\,\rho\underline{\ }g\,] \tag{3}$$

$\underline{v}\,.\,\underline{n} = v_o(\underline{x})$ on Γ^N
$p(\underline{x}) = p_o(\underline{x})$ on Γ^D
$\Gamma^N \cup \Gamma^D = \partial\Omega$
$\Gamma^N \cap \Gamma^D = \emptyset$
where
$\underline{n}$ unit normal vector.
v_o prescribed values of velocity.
p_o prescribed values of pressure on the boundary.
Γ^N Neumann boundary condition.
Γ^D Dirichilet boundary condition.

2.3. [V] or Weak form

Multiply both sides by w (test function) then integrate over the area (using Galerkin's formalism):

$$\int_\Omega w.\mathrm{div}\left[\frac{k}{\mu}\mathrm{grad}(p)\right]d\Omega = \int_\Omega w.\mathrm{div}\left[\rho\underline{g}\right]d\Omega, \forall w \tag{4}$$

Apply Green identity to the left side:

$$\int_\Omega \mathrm{div}\left[w\frac{k}{\mu}\mathrm{grad}(p)\right]d\Omega - \int_\Omega \mathrm{grad}[w].\mathrm{grad}[p]d\Omega = \int_\Omega w.\mathrm{div}\left[\rho\underline{g}\right]d\Omega \tag{5}$$

Apply divergence theorem to the first term in the left side:

$$\int_{\partial\Omega} w\frac{k}{\mu}\mathrm{grad}(p).\underline{n}d\Gamma - \int_\Omega \mathrm{grad}[w].\frac{k}{\mu}\mathrm{grad}[p]d\Omega = \int_\Omega w.\mathrm{div}\left[\rho\underline{g}\right]d\Omega \tag{6}$$

Then,

$$\int_\Omega \mathrm{grad}[w].\frac{k}{\mu}\mathrm{grad}(p).d\Omega = \int_{\partial\Omega} w\frac{k}{\mu}\mathrm{grad}[p].\underline{n}d\Gamma - \int_\Omega w.\mathrm{div}\left[\rho\underline{g}\right]d\Omega\,,\forall w \tag{7}$$

The first term in the right hand side can be simplified by assuming 2D problem and also take in consider:

$$\text{grad}[p] = \gamma_w \text{grad}[h] = \gamma_w \left[\frac{\partial h}{\partial x} \;\; \frac{\partial h}{\partial y}\right] = \gamma_w [0 \;\; 0] = 0 \tag{8}$$

Then, Eq. (8) becomes:

$$\int_{\Omega} \text{grad}[w].\frac{k}{\mu}\text{grad}(p).d\Omega = -\int_{\Omega} w.\text{div}\left[\rho \underline{g}\right] d\Omega\,, \forall w \tag{9}$$

Eq. (9) can be written as follows:

$$\int_{\Omega} \text{grad}[w].\frac{k\gamma_w}{\mu}\text{grad}(h).d\Omega = -\int_{\Omega} w.\text{div}[\underline{F}]d\Omega\,, \forall w \tag{10}$$

where h is the head of water. When the fluid is water, then: $\frac{k\gamma_w}{\mu} = 1.0$. Hence, Eq. (10) can be written:

$$\int_{\Omega} \text{grad}[w].\text{grad}(h).d\Omega = -\int_{\Omega} w.\text{div}[\underline{F}]d\Omega\,, \forall w \tag{11}$$

Eq. (11) is used in finite element formulation:

$$\text{LHS} = \int \text{grad}[w].\text{grad}(h).d\Omega = \int_{\Omega} \left(\underline{B}^T \Theta \underline{I}\right) vec \left[\underline{\underline{w^T}}\right].\left(\underline{B}^T \Theta \underline{I}\right) \text{vec}\left[\underline{\underline{h^T}}\right] d\Omega$$

$$= \text{vec}\left[\underline{\underline{w^T}}\right]^T \int_{\Omega} \left(\underline{B}^T \Theta \underline{I}\right)^T \left(\underline{B}^T \Theta \underline{I}\right) vec\left[\underline{\underline{h^T}}\right] d\Omega \tag{12}$$

$$\text{RHS} = -\int_{\Omega} w.\text{div}[\underline{F}]d\Omega = -\int_{\Omega} \left(\underline{N}\Theta\underline{I}\right) \text{vec}\left[\underline{\underline{w^T}}\right].\text{vec}\left[\underline{\underline{B^T}}\right]^T \text{vec}\left[\underline{\underline{F^T}}\right] d\Omega$$

$$= -\text{vec}\left[\underline{\underline{w^T}}\right]^T \int_{\Omega} \left(\underline{N}\Theta\underline{I}\right)^T \text{vec}\left[\underline{\underline{B^T}}\right]^T \text{vec}\left[\underline{\underline{F^T}}\right] d\Omega \tag{13}$$

From Eqs. (11) and (12):

vec $\left[\underline{\underline{w^T}}\right]^T$ will be dropped from both sides. Then, the full equation can be written:

$$\left[\underline{\underline{K}}\right]\left[\underline{U}\right] = \left[\underline{F}\right] \tag{14}$$

where

$$\left[\underline{\underline{K}}\right] = \int_{\Omega} \left(\underline{B}^T \Theta \underline{I}\right)^T \left(\underline{B}^T \Theta \underline{I}\right) d\Omega \qquad \text{(Known)}$$

$$\left[\underline{U}\right] = \text{vec}\left[\underline{\underline{h^T}}\right] \qquad \text{(Unknown)}$$

$$\left[\underline{F}\right] = -\int_{\Omega} \left(\underline{N}\Theta\underline{I}\right)^T \text{vec}\left[\underline{\underline{B^T}}\right]^T vec\left[\underline{\underline{F^T}}\right] d\Omega \qquad \text{(Known)}$$

2.4. Exact Solution of Laplace Equation

For the steady state flow in 2D homogenous, Laplace equation can be written as follows:

$$\nabla^2 h = \frac{\partial^2 h}{\partial^2 x} + \frac{\partial^2 h}{\partial^2 x} = 0 \tag{15}$$

The idealization of the steady state with given boundary conditions are shown in Fig. 1.

For the exact solution of the Laplace equation, separation of variables can be used:

$$h(x, y) = F(x)G(y) \tag{16}$$

$$\frac{1}{F}.\frac{d^2F}{dx^2} = -\frac{1}{G}.\frac{d^2G}{dy^2} = -k \tag{17}$$

Then,

$$\frac{d^2F}{dx^2} + kF = 0 \tag{18}$$

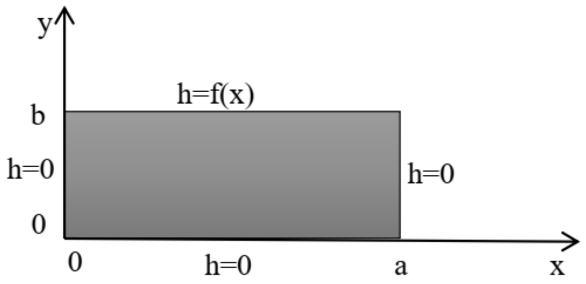

Fig. 1. Steady state dealization of 2D-homogenous Laplace quation.

From the left and right boundary conditions:

$$F(0) = 0, F(a) = 0 \Rightarrow k = \left(\frac{n \times \pi}{a}\right)^2 \tag{19}$$

$$F(x) = F_n(x) = \sin\left(\frac{n\pi}{a}x\right) \tag{20}$$

$$G(y) = G_n(y) = A_n e^{(n\pi y/a)} + B_n e^{(-n\pi y/a)} \tag{21}$$

By applying both bottom and top boundary conditions:

$$h(x, y) = \sum_{n=1}^{\infty} A_n^* \sin\left(\frac{n\pi x}{a}\right) \sinh\left(\frac{n\pi y}{a}\right) \tag{22}$$

$$A_n^* = \frac{2}{a \sinh(n\pi b/a)} \int_0^a f(x) \sin\left(\frac{n\pi x}{a}\right) dx \tag{23}$$

where n is number of points in the Fourier series.

3. RESULTS AND ANALYSIS

The description of the studied case can be shown in Fig. 2. The problem represents the seepage of water under sheet pile from upstream level to downstream level. Both exact and numerical solutions have been investigated using different Fourier points and number of nodes. The element numbering has started form the upper left side of the mesh where the node numbers are given in clock wise order.

Several trials have been investigated for the case study as shown in Table 1. All the studied trials have the same dimensions with width (a) and height (b) of 10 m. In addition, the upstream and downstream heads for all the trails are 5 m, and 1 m respectively. The variation of the head contours for both FEM and analytical solutions for the first trial (one point Fourier, nine nodes in *X* and *Y* directions) have shown in Fig. 3. In the FEM, the contours of the head distribution are concentrated on the upper left side where the high head in the upstream is located. However, in the exact solution; the contours of the head distribution are concentrated on the upper middle side in symmetrical shape.

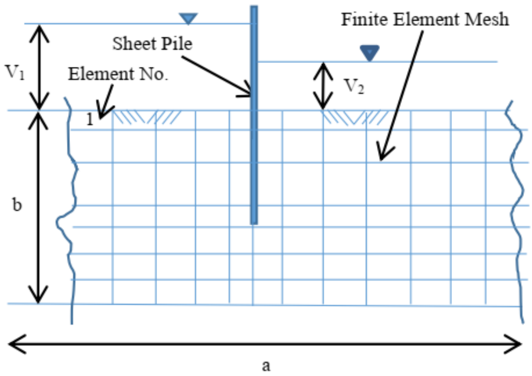

Fig. 2. General description of the case study.

Table 1
Details of the case study.

Trial no.	N (Fourier points)	a (m)	b (m)	V_1 (m)	V_2 (m)	X_{Seed} (no. nodes)	Y_{Seed} (no. nodes)
1	1	10	10	5	1	9	9
2	1	10	10	5	1	11	11
3	1	10	10	5	1	15	15
4	1	10	10	5	1	21	21
5	1	10	10	5	1	31	31
6	1	10	10	5	1	41	41
7	1	10	10	5	1	99	99
8	5	10	10	5	1	77	77
9	5	10	10	5	1	99	99
10	5	10	10	5	1	101	101

Similarly, the variation of the head contours for both FEM and analytical solutions for the second trial (one point Fourier, 11 nodes in *X* and *Y* directions) have shown in Fig. 4. In the FEM, the contours of the head distribution are a little smoother compared to FEM in the first trail that has lower number of nodes. Likewise, the variation of the head contours for both FEM and analytical solutions for the third trial (one point Fourier, 15 nodes in X and Y directions) have shown in Fig. 5. In the FEM, the contours of the head distribution are started to be smoother compared to FEM in the previous trails that have lower number of nodes. In addition, the variation of the head contours for both FEM and analytical solutions for the fourth trial (one point Fourier, 21 nodes in *X* and *Y* directions) have shown in Fig. 6. Smoother head contours distributions are observed for FEM compared to the previous trials.

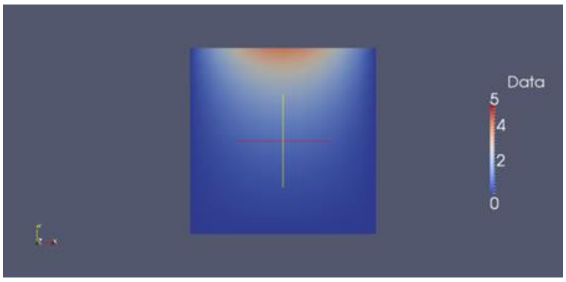

(a)

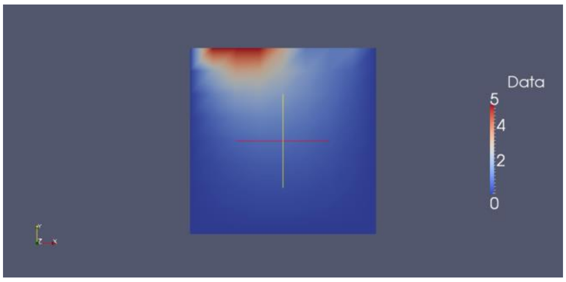

(b)

Fig. 3. Contours of head for trial 1, (a) Exact soultion, and (b) FEM.

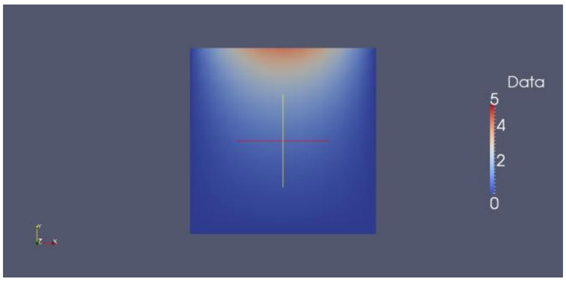

(a)

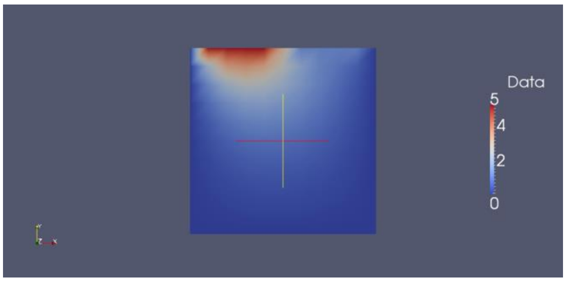

(b)

Fig. 4. Contours of head for trial 2, (a) Exact solution, and (b) FEM.

The variation of the head contours for both FEM and analytical solutions for the fifth, sixth, and seventh trials (one point Fourier; 31, 41, and 99 nodes in *X* and *Y* directions) have shown in Figs. 7- 9. As the numbers of nodes are increased in FEM, smoother head contours distributions are noticed.

The variation of the head contours for both FEM and analytical solutions for the eighth trial (five points Fourier;

77 nodes in *X* and *Y* directions) have shown in Fig. 10. In the FEM, the contours of the head distribution are concentrated on the upper left side where the high head in the upstream is located. In the exact solution, as the Fourier Points increased from 1 to 5; the contours of the head distribution are moved towards the region of high head in the upstream zone on the upper left side. The variation of the head contours for both FEM and analytical solutions for the ninth trial (five points Fourier; 99 nodes in *X* and *Y* directions) have shown in Fig. 11. As the numbers of nodes are increased in FEM, smoother head contours distributions are noticed. The variation of the head contours for both FEM and analytical solutions for the tenth trial (five points Fourier; 101 nodes in *X* and *Y* directions) have shown in Fig. 12. As the numbers of nodes are increased in FEM, smoother head contours distributions are noticed.

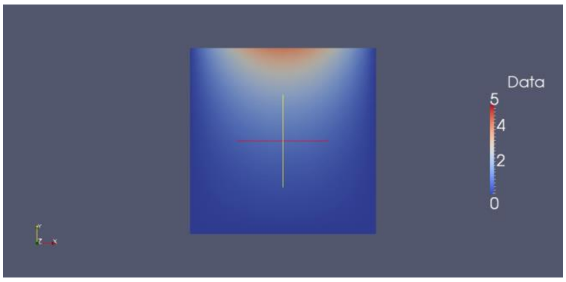

(a)

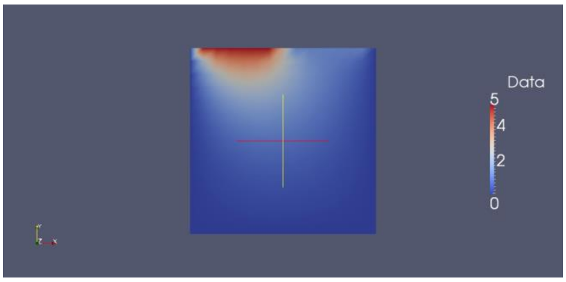

(b)

Fig. 5. Contours of head for trial 3, (a) Exact solution, and (b) FEM.

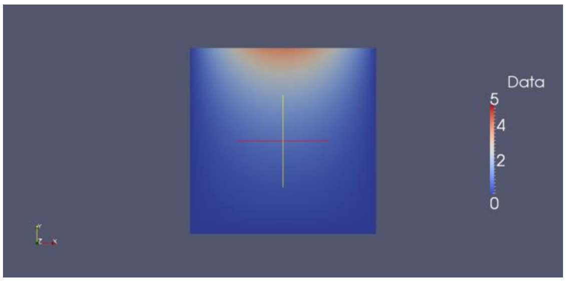

(a)

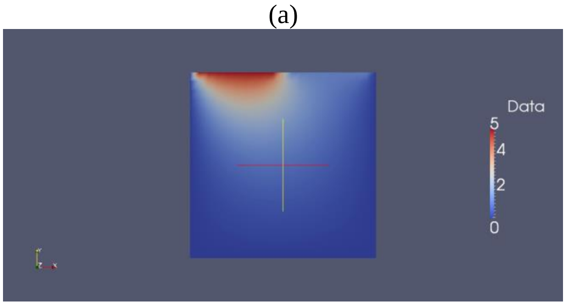

(b)

Fig. 6. Contours of head for trial 4, (b) Exact solution, and (b) FEM.

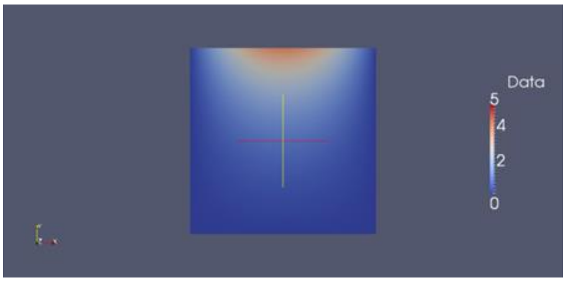

(a)

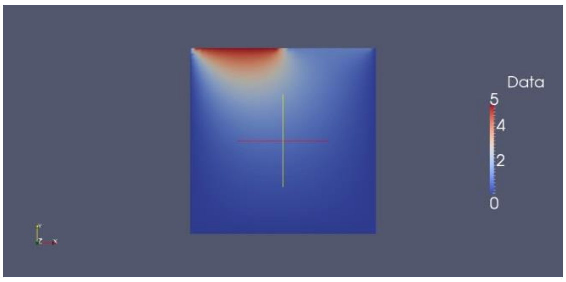

(b)

Fig. 7. Contours of head for trial 5, (a) Exact solution, and (b) FEM.

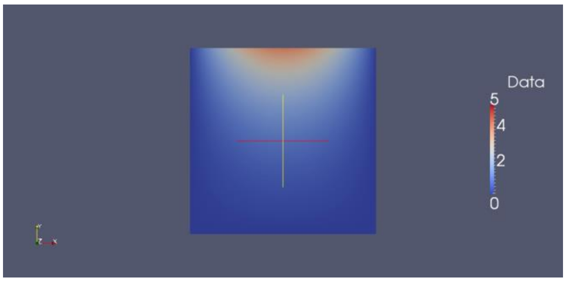

(a)

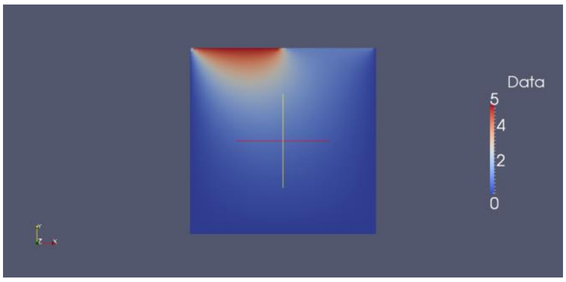

(b)

Fig. 8. Contours of head for trial 6, (a) Exact solution, and (b) FEM.

The variation of the total head with node number for both exact and FEM solutions using five nodes as total number of nodes in x and y directions is shown in Fig. 13. The FEM solution is very close to the exact solution in all the nodes with the 100% value prediction in the locations that has zero total head.

The variation of the absolute error of total head prediction with node number for both exact and FEM solutions using five nodes as total number of nodes in x and y directions is shown in Fig. 14. In most of the nodes, the FEM solution is very close to the exact solution with almost zero absolute error. However, in several nodes; there is a quite high absolute error prediction with the maximum value of 61% at node 22 (upper right side of the mesh).

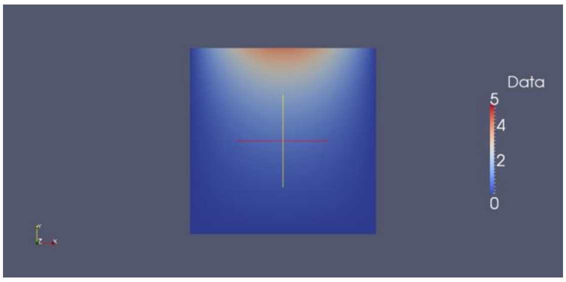

(a)

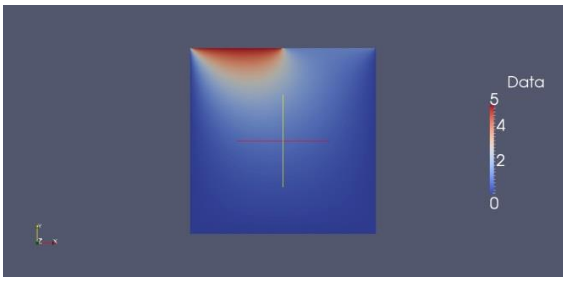

(b)

Fig. 9. Contours of head for trial 7, (a) Exact solution, and (b) FEM.

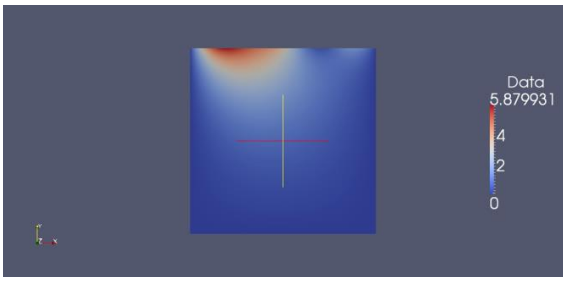

(a)

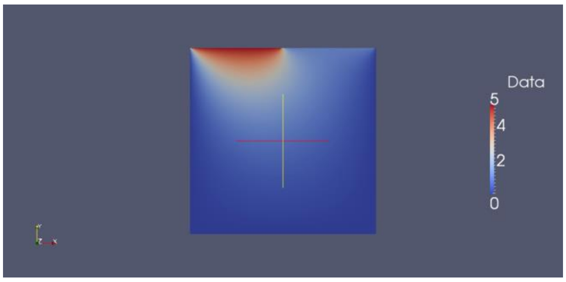

(b)

Fig. 10. Contours of head for trial 8, (a) Exact solution, and (b) FEM.

The variation of the total head with node number for both exact and FEM solutions using nine nodes as total number of nodes in x and y directions is shown in Fig. 15. With increasing the number of nodes, the FEM solution is very close to the exact solution in most of the nodes with the 100% value prediction in the locations that has zero total head.

The variation of the absolute error of total head prediction with node number for both exact and FEM solutions using nine nodes as total number of nodes in x and y directions is shown in Fig. 16. In most of the nodes, the FEM solution is very close to the exact solution with almost zero absolute error. Nevertheless, in several nodes; there is a quite high absolute error prediction with the maximum value of 61% at node 75 (upper right zone of the downstream).

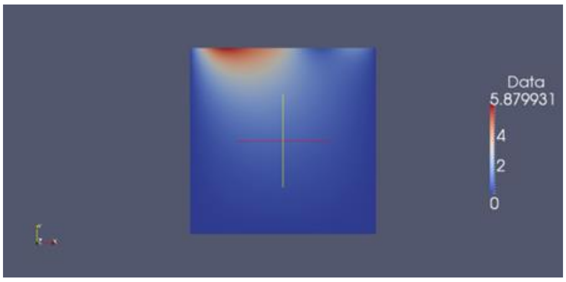

(a)

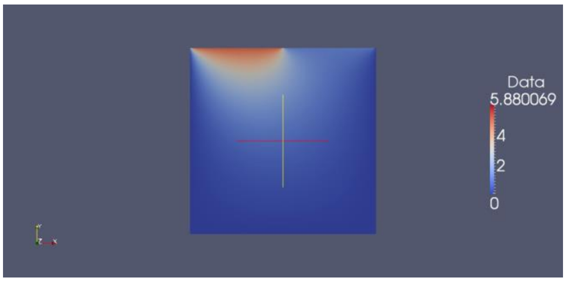

(b)

Fig. 11. Contours of head for trial 9, (a) Exact solution, and (b) FEM.

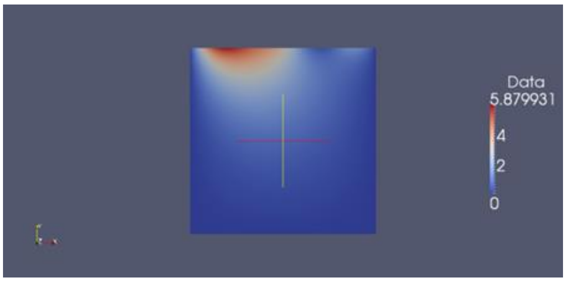

(a)

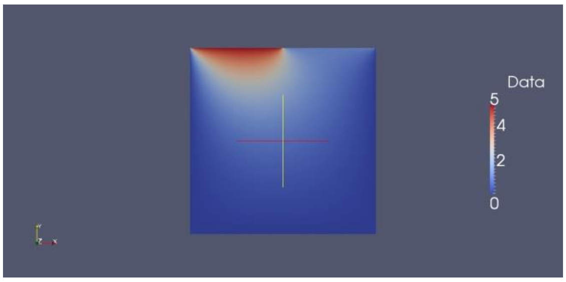

(b)

Fig. 12. Contours of head for trial 10, (a) Exact solution, and (b) FEM.

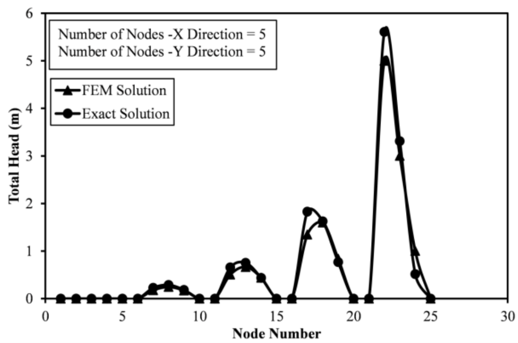

Fig. 13. Variation of total head with node number for both exact and FEM solutions (number of nodes in *X* and *Y* directions = 5).

The variation of the total head with node number for both exact and FEM solutions using 11 nodes as total number of nodes in *x* and *y* directions is shown in Fig. 17. With increasing the number of nodes, the FEM solution is very close to the exact solution in most of the nodes with the 100% value prediction in the locations that has zero total head.

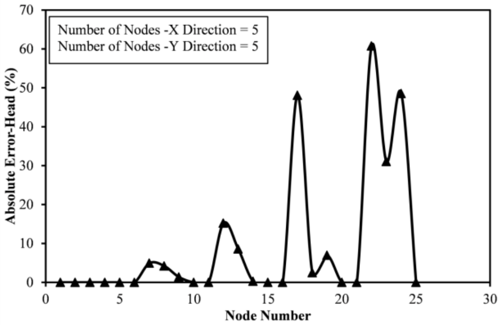

Fig. 14. Variation of absolute error with node number for total head (number of nodes in *X* and *Y* directions = 5).

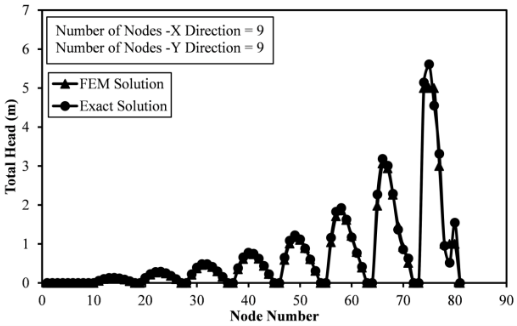

Fig. 15. Variation of total head with node number for both exact and fem solutions (number of nodes in *X* and *Y* directions = 9).

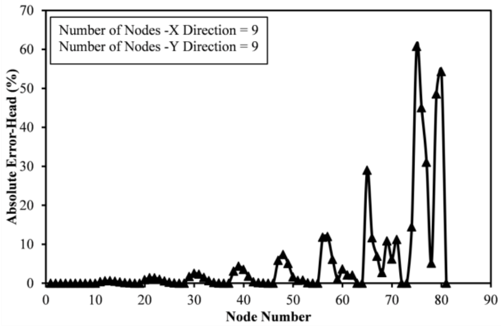

Fig. 16. Variation of absolute error with node number for total head (number of nodes in *X* and *Y* directions = 9).

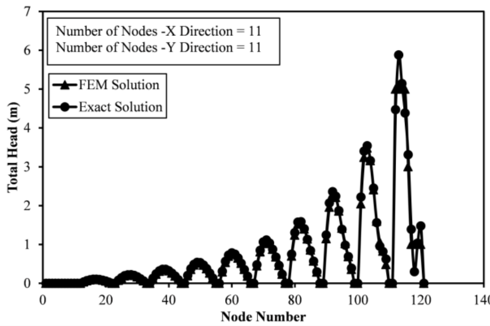

Fig. 17. Variation of total head with node number for both exact and fem solutions (number of nodes in *X* and *Y* directions = 11).

The variation of the absolute error of total head prediction with node number for both exact and FEM solutions using 11 nodes as total number of nodes in x and y directions is shown in Fig. 18. In most of the nodes, the FEM solution is very close to the exact solution with almost zero absolute error. Nevertheless, in several nodes; there is a quite high absolute error prediction with the maximum value of 88% at node 113 (upper right zone of the downstream).

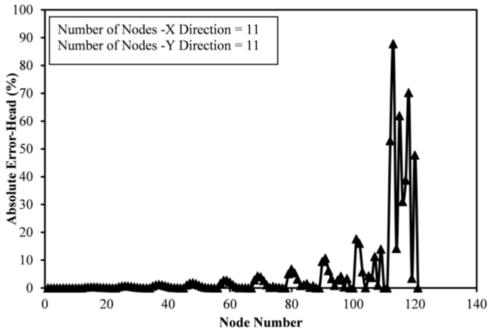

Fig. 18. Variation of absolute error with node number for total head (number of nodes in *X* and *Y* directions = 11).

4. CONCLUSIONS

In this study, an exact solution approach as Fourier series of the Laplace partial differential equation has been introduced to solve one of the geotechnical problems, the seepage of water under a sheet pile, which adopts also a finite element method. Even though of considering Fourier series an exact solution for the Laplace equation, it is originally an approximate procedure due to n points which cannot be infinite. The following results can be pointed out:

1- Both exact and finite element solutions have a good match in distribution over the studied area especially when the Fourier points are increased.
2- In general, the absolute errors of total head prediction are reasonable except in the top surface where the absolute error may reach 88% when the total number of nodes are 11 in both x and y directions.

REFERENCES

[1] Farid B, Naima B. Critical hydraulic head loss assessment for a circular sheet pile wall under axisymmetric seepage conditions. *Studia Geotechnica et Mechanica* 2011; **33** (4): 3–25.

[2] Terzaghi K. Theoretical soil mechanics. Wiley: New York; 1943.

[3] Suvasish M. Seepage analysis through foundation using FEM and Flownet. *The 12th International Conference of International Association for Computer Methods and Advances in Geomechanics* 2008; 1-6 October; Goa; India: 4175-4183.

[4] Hirani AN, Nakshatrala KB, Chaudhry JH. Numerical method for Darcy flow derived using discrete exterior calculus. *International Journal for Computational Methods in Engineering Science and Mechanics* 2015; **16**: 151–169.

[5] Liu GR, Dai KY, Nguyen TT. A smoothed finite element method for mechanics problems. *Computational Mechanics* 2007; **39** (6): 859–877.

[6] Esteban HZ, Pamela OF, Francisco RF. Some applications to mine geotechnical design using Matlab. *Matilde Salamanca 736 Piso 6 Providencia Santiago Chile*; 2007.

[7] Esteban HZ, Pamela OF, Francisco RF. Some applications to mine geotechnical design using Matlab. *Matilde Salamanca 736 Piso 6 Providencia Santiago Chile*; 2007.